

Start-Up and First Physics Results with the ATLAS Detector at the LHC

A. WILDAUER⁽¹⁾, ON BEHALF OF THE ATLAS COLLABORATION

⁽¹⁾ *IFIC, Apartado de Correos 22085, 46071 Valencia, Spain*

Summary. — An overview of the first data taking with the ATLAS detector at the Large Hadron Collider (LHC) is given. Data were collected in December 2009 during approximately ten days of running at a centre-of-mass energy of 900 GeV (and shortly at 2.36 TeV). An impressive amount of studies have been carried out by the ATLAS collaboration on these data. A small selection of results from detector performance and combined performance groups are presented as well as results from the first physics analysis of ATLAS on charged-particle multiplicities in 900 GeV collisions.

PACS 01.30.Cc – Conference proceedings.

PACS 13.85.-t – Hadron-induced high- and super-high-energy interactions.

1. – Introduction

An excerpt of detector performance and first physics results of the ATLAS collaboration using the 2009 data taking of the LHC [1] at 900 GeV centre-of-mass energy is presented. The ATLAS detector [2] at the LHC has been designed to study a wide range of physics topics at LHC energies. It covers almost the whole solid angle around the collision point with layers of tracking detectors, calorimeters and muon chambers.

The ATLAS inner detector has full coverage in ϕ and covers the pseudorapidity range ⁽¹⁾ $|\eta| < 2.5$. It consists of a silicon pixel detector (Pixel), a silicon microstrip detector (SCT) and a transition radiation tracker (TRT). These detectors cover a sensitive radial distance from the interaction point of 50.5-150 mm, 299-560 mm and 563-1066 mm, respectively, and are immersed in a 2 T axial magnetic field. The inner-detector barrel (end-cap) parts consist of 3 (2×3) pixel layers, 4 (2×9) double-layers of single-sided silicon microstrips with a 40 mrad stereo angle, and 73 (2×160) layers of TRT straws. These detectors have position resolutions of typically 10, 17 and 130 μm for the R- ϕ co-ordinate and, in case of the Pixel and SCT, 115 and 580 μm for the second measured

⁽¹⁾ Pseudorapidity is defined as $\eta = -\ln \tan(\theta/2)$

co-ordinate. A track from a particle traversing the barrel detector would typically have 11 silicon hits (3 pixel clusters and 8 strip clusters), and more than 30 straw hits.

High granularity liquid-argon (LAr) electromagnetic sampling calorimeters, with excellent performance in terms of energy and position resolution, cover the pseudorapidity range of up to $|\eta| = 4.9$. The hadronic calorimetry in the range $|\eta| < 1.7$ is provided by a scintillator-tile calorimeter, which is separated into a large barrel and two smaller extended barrel cylinders, one on either side of the central barrel.

The calorimeter is surrounded by the muon spectrometer. The air-core toroid system, with a long barrel and two inserted end-cap magnets, generates strong bending power in a large volume within a light and open structure. Multiple-scattering effects are thereby minimised, and excellent muon momentum resolution is achieved with three layers of high precision tracking chambers. The muon instrumentation includes, as a key component, trigger chambers with timing resolution of the order of 1.5-4 ns. The muon spectrometer defines the overall dimensions of the ATLAS detector.

2. – Data Taking and Trigger

ATLAS recorded approximately 538.000 collisions under LHC stable beam conditions (which means that it is safe for ATLAS to turn on the full inner detector). The integrated luminosity recorded by ATLAS during stable beams corresponds to $\approx 9 \mu\text{b}^{-1}$ with a systematic uncertainty of about 30%. The maximum peak luminosity as measured in ATLAS was $L \approx 7 \times 10^{26} \text{ cm}^{-2}\text{s}^{-1}$. The operational fraction of all ATLAS detector and trigger systems was close to 100% at all times.

The ATLAS detector has a three-level trigger system: Level 1 (L1), Level 2 (L2) and Event Filter (EF). The main physics trigger during the 2009 data taking relied on the L1 signals from the Beam Pickup Timing devices (BPTX) and the Minimum Bias Trigger Scintillators (MBTS). The BPTX are composed of beam pick-ups attached to the beam pipe at $z = \pm 175 \text{ m}$ from the centre of the ATLAS detector. The MBTS are mounted at each end of the detector in front of the liquid-argon end-cap calorimeter cryostat at $z = \pm 3.56 \text{ m}$.

3. – Detector and Combined Performance Plots

ATLAS has produced an impressive amount of results of detector and combined performance studies on the 2009 data at 900 GeV centre-of-mass energy. This section can only show a small selection of these results trying to span all detectors from the inner detector to the muon spectrometer.

The Pixel detector has an analogue read-out and can therefore measure the energy loss of traversing particles. Fig. 1(a) shows the energy loss versus the charge times the momentum of the traversing particles. The bands for protons, kaons and pions can clearly be seen. A cross-check has been done by reconstructing the decay of particles such as $\Lambda \rightarrow p\pi^-$ as shown in Fig. 3. When only plotting the energy loss for the decay product of the Λ (and $\bar{\Lambda}$) decay only the bands for protons and pions remain (see Fig. 1(b)).

The TRT has the capability to separate electrons and pions by measuring the photon radiation of the traversing particle. The intensity of this transition radiation is proportional to the Lorentz factor $\gamma = \frac{E}{m_0 c^2}$ of the traversing particle. Fig. 2(a) shows the probability to produce so called high threshold hits which are due to transition radiation in the TRT for data and Monte Carlo. Pions in the momentum range 1 - 10 GeV radiate far fewer photons than electrons in the same momentum range due to the large mass

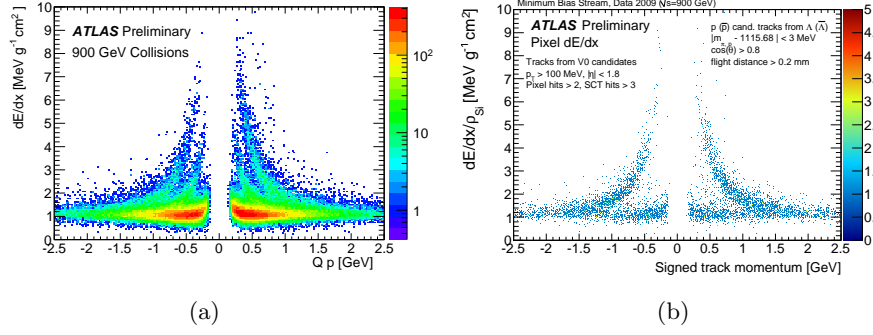


Fig. 1. – (a) Energy loss in the pixel detector for all reconstructed tracks. The bands for pions, kaons and protons are clearly visible. (b) A pre-selection of tracks using only the proton of $\Lambda \rightarrow p\pi^-$ (and \bar{p} of $\bar{\Lambda} \rightarrow \bar{p}\pi^+$) removes the kaon band.

difference between the two particles. A cross-check of this can be done by using identified electrons from photon conversions ($\gamma \rightarrow e^+e^-$). Fig. 2(b) shows the fraction of high threshold hits for all reconstructed tracks in data and Monte Carlo. The shaded area towards higher fractions of high threshold hits is entirely due to electrons from photon conversions.

The reconstruction of well known particle decays such as $K_S^0 \rightarrow \pi^+\pi^-$, $\Lambda \rightarrow p\pi^-$ or $\bar{\Lambda} \rightarrow \bar{p}\pi^+$ is a powerful tool to understand and validate the performance of the detector. Fig. 3 shows the reconstructed invariant mass spectra of the K_S^0 and the Λ . The mean values of the reconstructed particle mass for the K_S^0 , Λ and $\bar{\Lambda}$ (the latter is not shown) agree very well with the world average [3]. The widths of the distributions are in very good agreement between data and Monte Carlo. This underlines the good understanding of the detector (*e.g.* the material in the inner detector) at this early stage of data taking.

The electromagnetic calorimeter measures the energy of electrons and photons. Its response to single isolated tracks is a good measure for the understanding of the calorimeter and also of the material in the inner detector. Fig. 4 shows the energy deposited in the

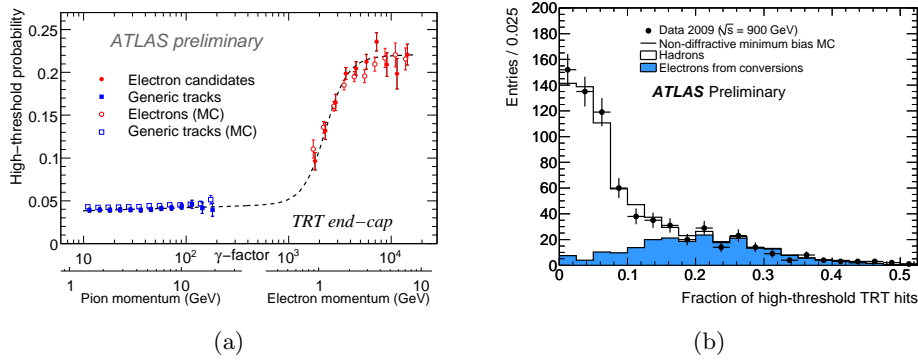


Fig. 2. – (a) The probability of a high-threshold hit in the TRT as a function of the Lorentz factor $\gamma = \frac{E}{m_0 c^2}$. (b) Fraction of high threshold hits in the TRT for all reconstructed tracks in data and Monte Carlo.

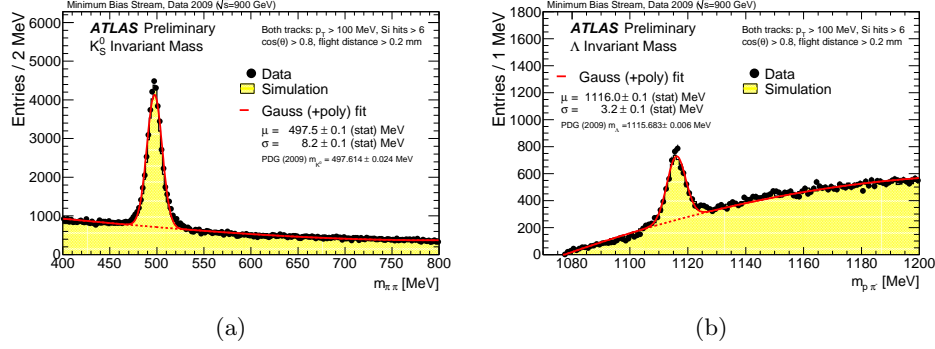


Fig. 3. – Reconstructed invariant mass spectra of (a) $K_S^0 \rightarrow \pi^+\pi^-$ and (b) $\Lambda \rightarrow p\pi^-$.

calorimeter over the momentum of a track as measured in the inner detector in the barrel region ($|\eta| < 0.8$) for isolated hadrons for data and Monte Carlo. The transverse momentum of all reconstructed tracks was required to be within the range 0.5 and 10 GeV. An isolation requirement of no other tracks within a cone in η and ϕ of 0.4 was made. The peak at zero is due to particles that stopped in the inner detector (*e.g.* due to hadronic interactions) and hence did not deposit any energy in the calorimeter. The agreement between simulation and data is remarkable and also reflects a good understanding of the material in the inner detector in the simulation.

The muon spectrometer will play an important role in triggering on interesting physics channels at higher centre-of-mass energies. However, already at $\sqrt{s} = 900$ GeV, where the cross sections for prompt muon production and decays such as $J/\Psi \rightarrow \mu^+\mu^-$ are very low around 50 muon candidates were reconstructed using the combined performance of the inner detector and the muon spectrometer. Fig. 5(a) shows the pseudorapidity and Fig. 5(b) the transverse momentum of these muon candidates. Reconstructed muon candidates are very forward (*i.e.* large $|\eta|$) and have rather low transverse momenta around several GeV (compared to what is expected at higher centre-of-mass energies).

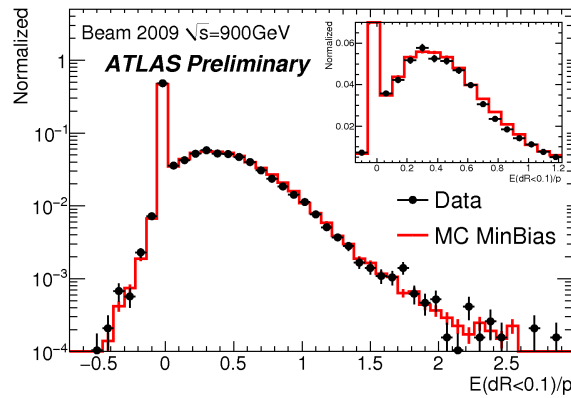


Fig. 4. – The energy deposited in the calorimeter over the momentum, as measured in the inner detector, of an isolated track.

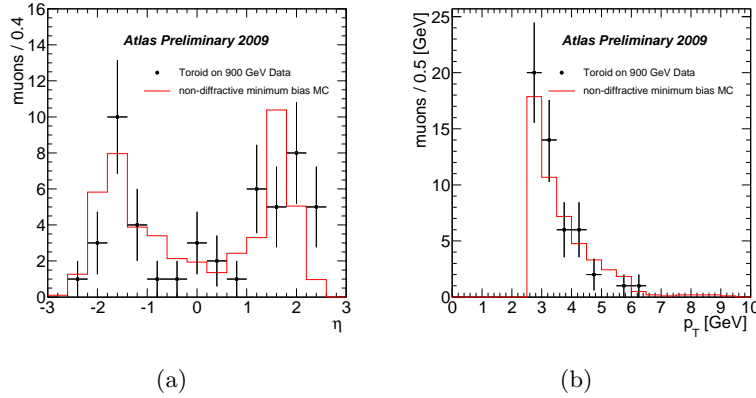


Fig. 5. – Muon candidates reconstructed in the inner detector and muon spectrometer as a function of (a) pseudorapidity, and (b) transverse momentum.

4. – Charged-Particle Multiplicities at $\sqrt{s} = 900$ GeV

The study of charged-particle multiplicities at a centre-of-mass energy of 900 GeV is described in the first physics paper released by ATLAS [4]. The measurement of charged-particle multiplicities in proton-proton reactions constrains phenomenological models of soft Quantum Chromodynamics (QCD) and therefore is an important ingredient for future studies of high transverse momentum phenomena at the LHC.

The charged-particle multiplicities were measured at 900 GeV within the kinematic range of $|\eta| < 2.5$, $p_T > 500$ MeV and the requirement of one charged-particle within this range. The data were presented as fully corrected inclusive-inelastic distributions at the particle level:

$$\frac{1}{N_{\text{ev}}} \cdot \frac{dN_{\text{ch}}}{d\eta}, \quad \frac{1}{N_{\text{ev}}} \cdot \frac{1}{2\pi p_T} \cdot \frac{d^2 N_{\text{ch}}}{d\eta dp_T}, \quad \frac{1}{N_{\text{ev}}} \cdot \frac{dN_{\text{ev}}}{dn_{\text{ch}}} \quad \text{and} \quad \langle p_T \rangle \text{ vs. } n_{\text{ch}},$$

where N_{ev} is the number of events with at least one charged-particle inside the selected kinematic range, N_{ch} is the total number of charged-particles, n_{ch} is the number of charged-particles in an event and $\langle p_T \rangle$ is the average p_T for a given number of charged-particles. A primary charged-particle was defined as a particle with a mean lifetime of $\tau < 0.3 \times 10^{-10}$ s which is either directly produced in the pp collision or stems from a subsequent decay of a particle with a shorter lifetime.

The trigger used for this analysis was a combination of the BPTX and the MBTS as described in section 2. The MBTS trigger was configured to require one hit above threshold from either side of the detector (so called: single-arm trigger). The efficiency of this trigger was derived from data and was obtained by comparison with an independent prescaled L1 BPTX trigger which was filtered to obtain inelastic interactions by loose inner detector requirements at L2 and EF. The primary vertex reconstruction efficiency was also derived from data and was measured with respect to the L1 MBTS trigger. It was found to only depend on the number of reconstructed tracks per event and, in case of only one reconstructed track also on η of the track. Fig. 6 shows trigger and primary vertex reconstruction efficiency as a function of the number of reconstructed tracks per event. The efficiencies are close to 100% except for events with very few reconstructed

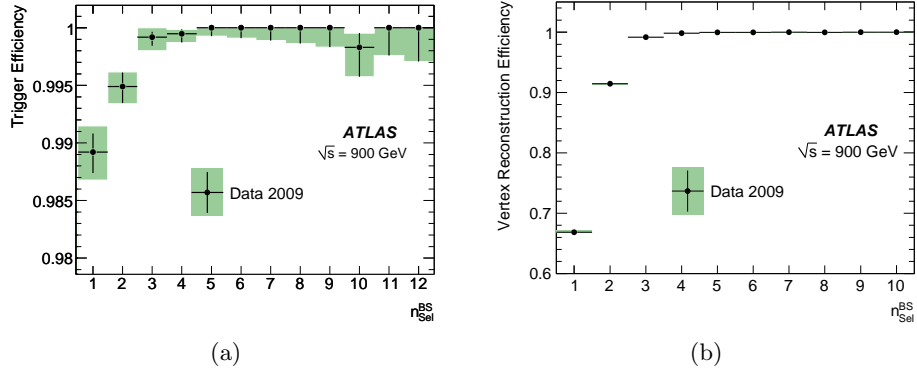


Fig. 6. – (a) Trigger and (b) primary vertex reconstruction efficiency as derived from data versus the number of reconstructed tracks ($n_{\text{Sel}}^{\text{BS}}$). The bands include statistical and systematic uncertainties.

tracks. The background contributions from cosmic-rays and beam-induced background were measured to be of the order of 10^{-4} and 10^{-6} , respectively. The contribution from secondary tracks which have been reconstructed as primary tracks was estimated to be $(2.20 \pm 0.05(\text{stat.}) \pm 0.11(\text{syst.}))\%$.

The track-reconstruction efficiency was derived from Monte Carlo. The understanding of and the agreement between Monte Carlo and data concerning track-reconstruction in the inner detector had therefore to be studied in great detail. It was found that the global uncertainty on the amount of material in the inner detector was less than 10%. The track-reconstruction efficiency versus η and p_T as derived from Monte Carlo is shown in Fig. 7.

All distributions were corrected for trigger, primary vertex and track-reconstruction efficiency. The final corrected distributions of primary charged-particles are shown in Fig. 8, where they are compared to predictions of models tuned to a wide range of

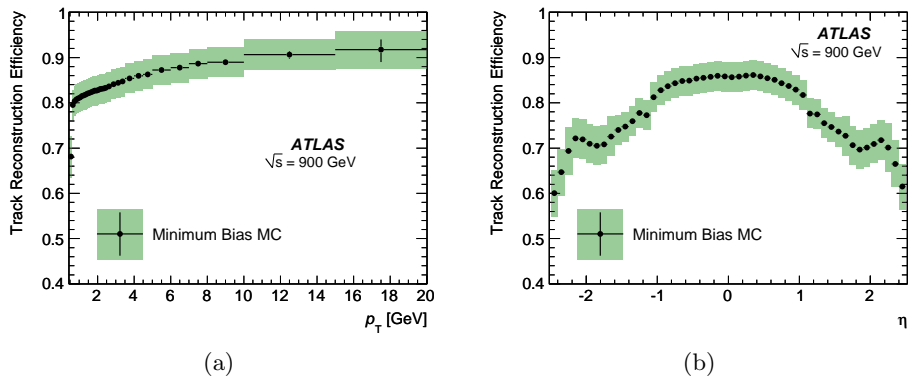


Fig. 7. – The track-reconstruction efficiency as derived from Monte Carlo is shown versus pseudorapidity (a) and transverse momentum (b). The bands include statistical and systematic uncertainties.

measurements. The charged-particle pseudorapidity density is shown in Fig. 8(a). It is measured to be approximately flat in the range $|\eta| < 1.5$. The charged-particle multiplicity per event and unit of pseudorapidity at $\eta = 0$ is measured to be $1.333 \pm 0.003(\text{stat.}) \pm 0.040(\text{syst.})$, which is 5–15% higher than the Monte Carlo model predictions. The particle density is found to drop at higher values of $|\eta|$. The N_{ch} distribution in bins of p_{T} is shown in Fig. 8(b) and is constructed by weighting each entry by $1/p_{\text{T}}$. The multiplicity distribution as a function of n_{ch} is shown in Fig. 8(c) and finally Fig. 8(d) shows the average p_{T} as a function of n_{ch} . The latter is found to increase with increasing n_{ch} and a change of slope is observed around $n_{\text{ch}} = 10$. This behaviour was already observed by the CDF experiment in pp collisions at 1.96 TeV [5].

5. – Conclusion

First performance and physics results from the ATLAS detector at the LHC are presented. An impressive amount of detector and combined performance results have been produced and only a small excerpt could be shown here. These studies show that the ATLAS detector is performing extremely well. The many years of preparation from test-beam, cosmic-ray, and Monte Carlo studies have paid off, ensuring such a successful start to data taking. The first physics measurements of inclusive-inelastic primary charged-particle multiplicities in 900 GeV proton-proton collisions have been presented. The charged-particle multiplicity per event and unit of pseudorapidity at $\eta = 0$ is measured to be $1.333 \pm 0.003(\text{stat.}) \pm 0.040(\text{syst.})$, which is 5–15% higher than the Monte Carlo model predictions.

REFERENCES

- [1] EVANS L., (ED.) and BRYANT P., (ED.), *JINST 3 (2008) S08001*, (LHC Machine)
- [2] AAD G., ET AL., ATLAS COLLABORATION, *JINST 3 (2008) S08003*, (The ATLAS Experiment at the CERN Large Hadron Collider)
- [3] AMSLER C., ET AL., *Physics Letters B667, 1 (2008)*, (The Review of Particle Physics)
- [4] AAD G., ET AL., ATLAS COLLABORATION, *Physics Letters B688, 1 (2010)*, (Charged-particle multiplicities in pp interactions at $\sqrt{s} = 900$ GeV measured with the ATLAS detector at the LHC)
- [5] ABE F., ET AL., CDF COLLABORATION, *Phys. Rev. D 41 (1990) 2330*, (Pseudorapidity distributions of charged-particles produced in $\bar{p}p$ interactions at $\sqrt{s} = 630$ and 1800 GeV)

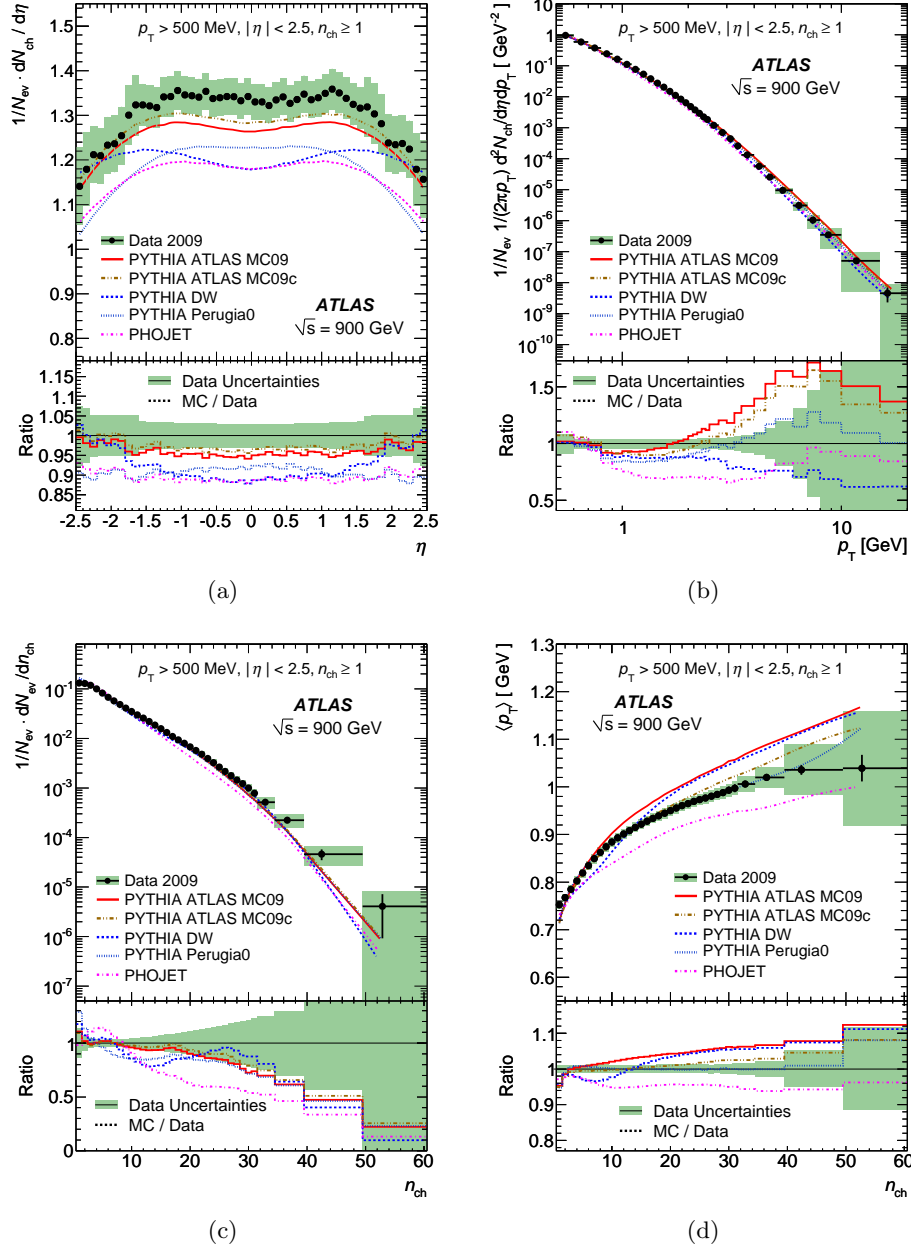


Fig. 8. – Inclusive-inelastic distributions of primary charged-particles at a centre-of-mass energy of $\sqrt{s} = 900$ GeV, in the kinematic range $p_T > 500$ MeV, $|\eta| < 2.5$ and the requirement of one charged-particle within this range.